Materials Chemistry and Physics 323 (2024) 129633

Contents lists available at ScienceDirect

Materials Chemistry and Physics

journal homepage: www.elsevier.com/locate/matchemphys

Quantitative modeling of oxide growth in plasma electrolytic oxidation of titanium

Kingsley Ochiabuto, Hunter Pitts, Ye Cao, Efstathios Meletis *

Department of Material Science and Engineering, University of Texas at Arlington, Arlington, TX, 76019, USA

HIGHLIGHTS

- Experimentally informed computational model for oxide growth predictions for PEO.
- Linear relationship discovered between the PEO model parameters and applied voltage.
- Model requires data from only two experiments at different applied voltages.
- Excellent agreement between the model and experimental measurements.

ARTICLE INFO

Keywords:
Plasma electrolytic oxidation
Titanium
Curve fitting
Potentiostatic
Oxide growth

ABSTRACT

Plasma electrolytic oxidation (PEO) has been extensively applied in the past to improve tribological properties of titanium and its alloys allowing their widespread use in industrial applications. However, the complete PEO mechanism of action remains unclear. While there are several mathematical models providing useful insights into the PEO process, they do not fully incorporate the effect of applied potential on the outcomes of PEO. In this work, we develop an experimentally informed computational model by expanding on the dielectric breakdown model. We incorporate experimental data to extract key parameters, exploring the iterative dependency of the oxide thickness and ionic current density to predict the oxide growth at various applied external voltages. The model reproduces the PEO process at different potentiostatic conditions and the simulation results for the oxide coating thickness over time is in good agreement with the experimental data, validating the application of Faraday's law and Pyun and Hong's model in describing the coating growth kinetics for the PEO process (Dehnavi et al., 2014/07/25/ 2014; Arrabal et al., 2009/05/30/ 2009; Rakoch et al., 2006/03/01 2006; Ma et al., 2017/10/10/ 2017; Pyun and Hong, 1992/02/01/ 1992; Caire et al., 2007/02/07 2007) [1-6].

1. Introduction

Titanium and its alloys have good biocompatibility, high corrosion resistance, high melting point, low density, and high strength-to-weight ratio. These properties are highly sought after in a wide range of industries, such as aerospace, medical devices, and sports equipment among others [7–9]. Unfortunately, the historically poor wear resistance, low hardness, and high surface contamination sensitivity of titanium have traditionally hindered its widespread use in industrial applications. Given the rising demand for titanium and its alloys, addressing these drawbacks has become a crucial area of research [10–15].

Researchers have embarked on a quest to address the aforementioned property limitations of titanium by investigating different approaches such as surface coatings/treatments, heat treatments, and alloying [16,17]. Several surface treatment techniques have been studied such as anodization, Plasma Electrolytic Oxidation (PEO), ion nitriding, shot peening, Physical Vapor Deposition (PVD), Chemical Vapor Deposition (CVD), among others [18–23]. Of these, PEO offers several advantages due to its low cost, excellent adhesion strength, and low environmental impact [24–27].

PEO involves the application of a high voltage to the metal surface in an electrolyte solution, creating a plasma discharge [8,25,28–30]. Numerous investigations have been conducted to explore the impact of electrolyte composition [31–33], temperature [34], electrical modes [35–38], and additives [39–44] on the characteristics of the produced

* Corresponding author.
E-mail address: meletis@uta.edu (E. Meletis).

https://doi.org/10.1016/j.matchemphys.2024.129633
Received 4 February 2024; Received in revised form 18 May 2024; Accepted 18 June 2024
Available online 25 June 2024
0254-0584/Published by Elsevier B.V.

PEO coatings [29,43]. Despite the progress made thus far, the complete mechanism of PEO remains not fully understood, primarily due to the challenges in probing the transient plasma discharges occurring on the material surface during treatment [1,2]. Obtaining a comprehensive understanding of the PEO mechanism is crucial for producing coatings with desirable characteristics suitable for a wide range of new applications.

Several models have been proposed to fundamentally understand the PEO process, including the barrier model, current model, discharge model, and dielectric breakdown model [1–5]. While these models have provided useful insights into various PEO phenomena, they do not fully incorporate the effect of applied potential on the outcomes of PEO [1,35,43]. In this work, we develop an experimentally informed computational model by expanding on the dielectric breakdown model [6]. We incorporate experimental data to extract key parameters, exploring the iterative dependency of the oxide thickness and ionic current density to predict the oxide growth at various applied external voltages.

2. Modelling and simulation

PEO can be conducted under several conditions, potentiodynamic, potentiostatic, galvanodynamic, galvanostatic, bipolar, etc. [4,8,38]. The galvanostatic and potentiostatic conditions are illustrated in Fig. 1. The PEO process can be categorized into several stages, each characterized by distinct phenomena. At the initial stage (stage 1), the cell voltage experiences a rapid and linear increase. This stage involves conventional anodization producing a thin insulating film and is accompanied by vigorous gas evolution. Eventually, the voltage reaches a critical value, referred to as the breakdown voltage, which leads to dielectric breakdown at weak points within the oxide film. Simultaneously, a multitude of fine, uniform, micro-discharges emerge on the surface, signifying the presence of sparks. These sparks and the formation of discharge channels are pivotal in the formation of the coating. Following the occurrence of the breakdown, the voltage increases gradually (stage 2), and the growth rate of the oxide film slows down. This phenomenon is attributed to the simultaneous processes of coating growth and dissolution. In stage 3, the micro-discharges become more intense and persist for longer duration, while their spatial density decreases. In stage 4, the rate of voltage further decreases, and the sparks intensify, but their population diminishes. Similar stages to those in the galvanostatic case are also present in the potentiostatic case that is characterized by a current decay over time, Fig. 1.

The equivalent circuit of the PEO process as proposed by Rakoch *et al.* [3] is shown in Fig. 2. The total current (I_t) passing through the system is split into two processes, (a) the electronic current (I_e) passing through the discharge channels, generating oxygen and plasma and (b) the ionic current (I_i) passing through the coating, generating oxide growth. R_c, R_d, and R_{el} are the resistance of the coating, discharge channel, and electrolyte, respectively. At any instant of time t, the total current I_t at the anode can be described by:

$$I_t = I_i + I_e \tag{1}$$

For the potentiostatic case, the potential distribution over the electrochemical cell as shown in Fig. 3 is described by:

$$V_{applied} = V_{m/c} + V_c + V_{c/e} \tag{2}$$

In the given expression, $V_{applied}$ denotes the applied potential. Additionally, $V_{m/c}$, V_c and $V_{c/e}$ correspond to the potential drops at the interface between the metal and the film, across the oxide coating, and at the interface between the film and the electrolyte, respectively.

To model the process based on this equivalent circuit, some

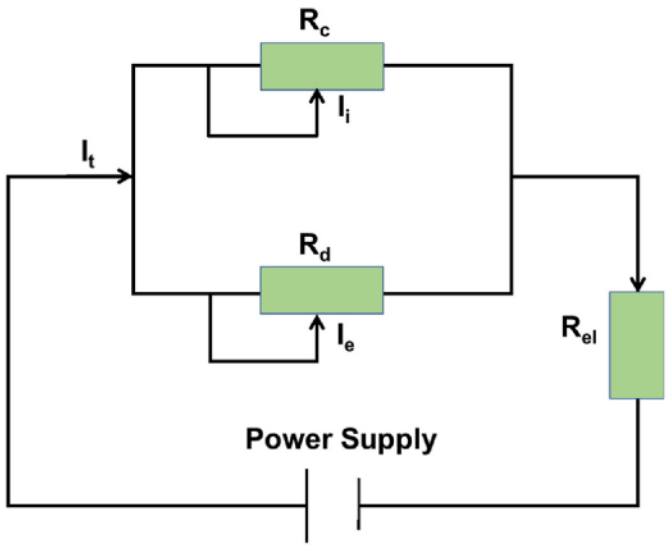

Fig. 2. PEO process simplified equivalent circuit.

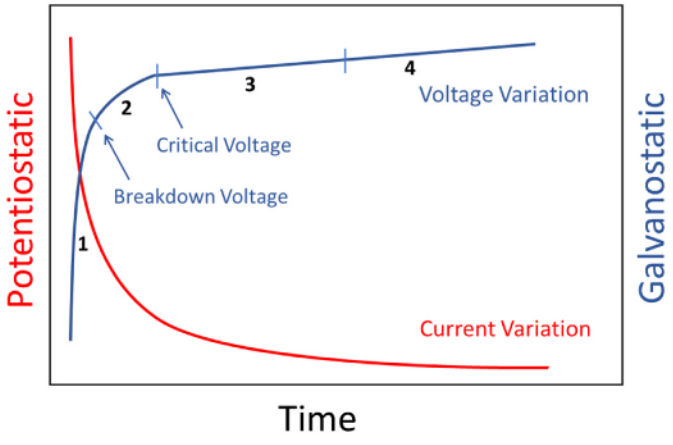

Fig. 1. Illustration of PEO stages and voltage or current variation with time under galvanostatic and potentiostatic control, respectively.

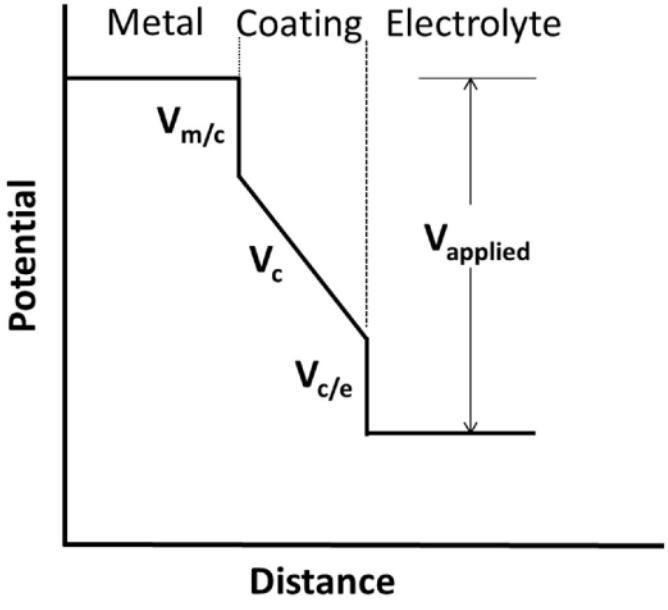

Fig. 3. Schematic illustration of the electric potential profile from anode to cathode.

assumptions were made.

- It is hypothesized that the plasma discharges originate from the bottom of the pores generated in the coating by the microdischarges, and the length of the discharge channel is equal to the thickness of the coating.
- PEO coating is composed of the crystalline phase of the oxide only.
- Potential drop is negligible at the metal electrodes. All the potential drops were at the metal/coating, coating, coating/electrolyte, and electrolyte/electrode interface, Fig. 3.
- Heat loss is negligible in the system.

The modeling presented in this paper is based on the more challenging case of PEO under potentiostatic control. The PEO experiments were conducted on rectangular 25 mm × 15 mm × 0.5 mm samples of commercially pure Titanium in an electrolyte of 0.02 M KOH and 0.01 M $K_4P_2O_7$. The particular electrolyte was also used in our previous PEO study [29] under constant current density allowing direct comparison between the two different modes of PEO processing of pure Ti. Tests were conducted for various time intervals at three different applied voltages, 450 V, 400 V, and 350 V and the current decay over time was recorded. The coating thickness was measured from sample cross sections using scanning electron microscopy and used as input in the model. A typical scanning electron micrograph of a sample cross section is shown in Fig. 4.

To provide a good depiction of the growth of the oxide coating on Ti during PEO, it is essential to understand the reactions taking place on the substrate and their kinetics. PEO coating formation can be simplified as a two-step process. In the first step, anions are generated at the interface between the oxide and the electrolyte. This process occurs due to the dissociation of adsorbed water, resulting in the formation of anions. Simultaneously, oxide formation commences through the migration of Ti^{4+} at the interface between the metal and the oxide. The second step is film formation taking place at the electrode/electrolyte interface when the concentrations of those ions reach a critical value [39].

$$Ti \rightarrow Ti^{4+} + 4e^{-} \text{ metal / oxide interface} \tag{3}$$

$$4OH^{-} \rightarrow O_2\uparrow + 2H_2O + 4e^{-} \text{ discharge channel} \tag{4}$$

$$Ti^{4+} + 4OH^{-} \rightarrow TiO_2 + 2H_2O \text{ oxide/electrolyte interface} \tag{5}$$

$$Ti^{4+} + 2(PO_4)^{2-} \rightarrow Ti(PO_4)_2 \text{ oxide/electrolyte interface} \tag{6}$$

The ionic current I_i represents the current of titanium dissolution, which corresponds to the electrode kinetics of the dissolution of titanium Eq. (3), and I_e is the current responsible for oxygen evolution and driving discharges, which describes the electrode kinetics of the oxygen release under the effect of electric field Eq. (4). The migration of Ti^{4+} and the presence of anions at the respective interfaces contributes to the growth of the oxide film. Eqs. (5) and (6) are considered chemical reactions that contribute to the growth of PEO coating on Ti surfaces.

The calculation of the reaction rate of the electrode surface ($R_{x,y}$) for each species in Eqs. (3) and (4) is determined in accordance with Faraday's law Eq. (7)

$$R_{x,y} = \frac{n_x J_i}{F q_y} \tag{7}$$

where q_y is the number of electrons exchanged during the formation reaction, n_x is the stoichiometric coefficient, F is Faraday's constant and J_i is the ionic current density.

In our analysis of the surface reaction, we have simplified the growth of the plasma electrolytic oxidation coating by considering it one-dimensional in the direction perpendicular to the metal sample surface. We assume that all titanium ions actively participate in the formation of the PEO coating. Additionally, we consider that there is an excess of anions available in the electrolyte, leading us to identify the availability of Ti^{4+} as the limiting factor for oxide growth. The limitation caused by the availability of Ti^{4+} and its influence on the growth rate of the oxide layer is depicted in Eqs. (8) and (9).

$$R_i = R_{TiO_2} = R_{Ti^{4+}} \text{ limiting reaction species} \tag{8}$$

The growth rate for the oxide layer is computed as:

$$G_{TiO_2} = \frac{R_{TiO_2} M_{TiO_2}}{\rho_{TiO_2}} \tag{9}$$

where M_{TiO_2} is the molar mass and ρ_{TiO_2} is the density of the TiO_2 coating.

The total coating thickness L is given in Eq. (10):

$$L = L_0 + \int_0^t G_{TiO_2} \tag{10}$$

where L_0 is the thickness of the passive layer on the metal surface.

The following equation as derived by Pyun and Hong [5] establishes a theoretical relationship between the ionic current density J_i contributing to oxide growth and the coating thickness (L):

$$J_i = \frac{P[\exp(nZL) - Q\exp(-nZL)]}{\exp(nZL) - 1} \tag{11}$$

where $Z = F\varepsilon/RT$.

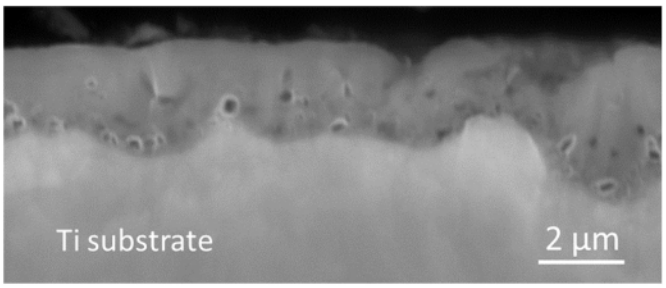

Fig. 4. Scanning electron micrograph of a cross section of a sample that was processed at 450 V for 100 s.

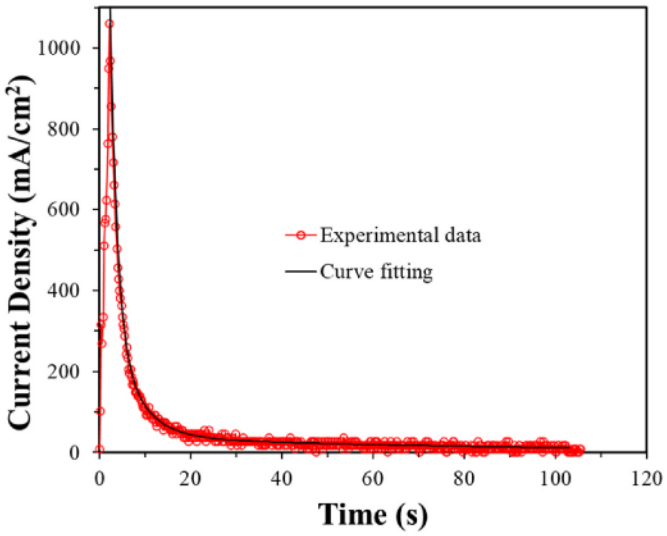

Fig. 5. Experimental data and corresponding fitting curve for total current density versus time at 450 V.

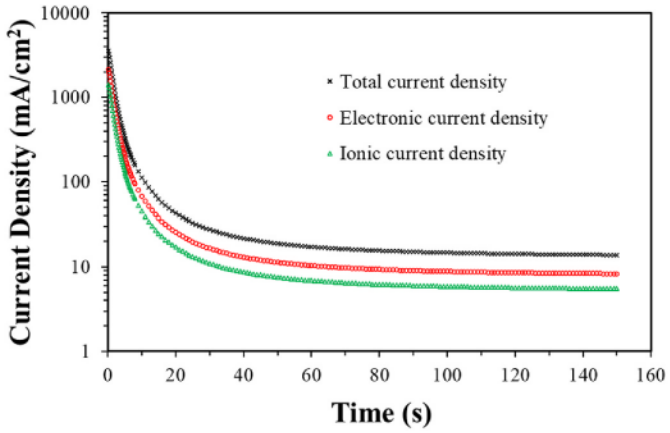

Fig. 6. A comparison of the total, ionic and electronic current densities over 100 s time interval at 450 V.

Here P, Q, and ε are constants for a certain experiment and are determined by the polynomial least-squares procedure. Also, n, F, R, and T are the charge number of Ti cations, Faraday's constant, gas constant and electrolyte's absolute temperature, respectively. The fitting procedure to solve Eq. (11) uses 40 % of the total current density and this was determined by iteratively solving for different ionic current densities as a percentage of total current density. The best solution obtained was for ionic current density as 40 % of total current density. A typical total current density decay with time measured experimentally at an applied potential of 450 V, and a generic fitting curve is shown in Fig. 5. A depiction of the ionic current density as 40 % of the total current density at 450 V is shown in Fig. 6.

3. Simulation results and discussion

To model the PEO process, we experimentally examined the time-dependent evolution of the thickness of the PEO coatings on the surface of Titanium under different potentiostatic conditions. Fig. 5 hence shows the evolution of the total current density upon the treatment time during the potentiostatic PEO processing. During the process, the voltage is raised fast above the breakdown voltage (285 V) of the oxide coating on the Titanium in the first 2 s and maintained at the desired potentiostatic conditions, i.e., 450 V, 400 V, and 350 V in our study. The

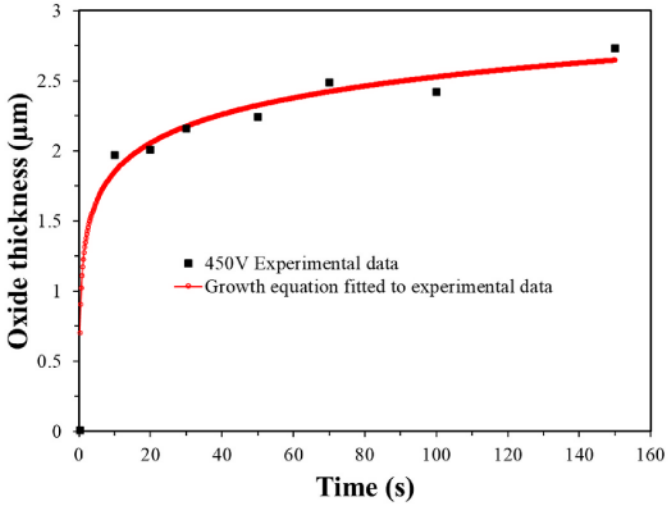

Fig. 7. Experimental oxide thickness data and the corresponding fitting curve.

Table 1
A summary of important parameters used for the computation.

Physical parameters	Value	Unit	Description
T	293	K	Temperature
Q_{el}	1.5	S/m	Electrolyte conductivity
$M(TiO_2)$	79.87	g/mol	Oxide molar mass
$\rho(TiO_2)$	4.23	g/cm^3	Oxide density
L_0	10	nm	Passive oxide thickness
$n(Ti^{4+})$	1		Stoichiometric coefficient (Ti^{4+})
$n(OH^-)$	4		Stoichiometric coefficient (OH^-)
$q(Ti^{4+})$	4		Number of electrons exchanged (Ti^{4+})
$q(OH^-)$	1		Number of electrons exchanged (OH^-)

current density variation in these first 2 s is almost linear and assumed to result in conventional anodization. The PEO is assumed to commence after this linear part of the current density evolution. To determine a relationship between the total current density and processing time, a mathematical decay curve is fitted to this experimental data. The equation of this fitted curve becomes an input in our study.

Our simulation is based on the assumption that the overall current density comprises two distinct elements: the ionic current density and the electronic current density [29]. The ionic current governs the growth of oxide, while the electronic current density is responsible for plasma discharges [4]. Fig. 6 illustrates trends of the total current density (depicting both the ionic and the electronic current density) at 450 V, as computed in the modeling process over a 150-s interval. Under potentiostatic conditions, the current density at the anode declines quickly within the initial few seconds after voltage application. At 10 s, it diminishes by 80 % of its initial magnitude, and by 50 s, most of the decay (95 %) has taken place primarily due to the formation of the PEO coating and its relatively high ohmic film resistance. A similar decay transient of the current density is depicted in Pyun and Hong's model [5]. Our average ionic current density constituted 40 % of the total current density which is similar to what was reported in Ma et al.'s work that, the average ionic current density constitutes 35 % of the total current density for the PEO of AM50 Mg alloy in KOH and Na_2PO_4 electrolyte [4] (see Table 1).

To explore the iterative dependency of the oxide thickness and ionic current density to predict the oxide growth at various applied external voltages, we first employ the model (Eq. (11)) proposed by Pyun and Hong [5] to establish the relationships between ionic current density and the oxide coating thickness. Oxide coating thickness, often expressed as $L = \alpha + \beta\, ln(t)$, where α, β, and t denote the initial oxide thickness, oxide growth rate, and time respectively, has been discussed in various works [4,5]. This is the generic mathematical expression of Eq. (10). In our study, we fitted the expression for L to our experimental oxide thickness, as illustrated in Fig. 7. Here, α was 10 nm thick and the final coating thickness (L) was measured when the treatment time was 100 s. An expression for β was then derived which satisfies the equation $L = \alpha + \beta\, ln(t)$. To solve model Eq. (11), parameters P, Q, and ε were determined through polynomial least square curve fitting of the ionic current density under three potentiostatic conditions: 450 V, 400 V, and 350 V. The outcomes as presented in Table 2 indicate that under given bias, the values for P, Q, and ε remain almost constant at different time intervals, underscoring the robustness of our solution. Using the optimal solutions for P, Q, and ε corresponding to the different potentiostatic conditions, we then described these parameters as functions of voltage (Fig. 8). Below are the expressions:

$$P = [0.0081V + 0.5437]\ (mA/cm^2) \tag{12}$$

$$Q = 2.098\text{x}10^7\ exp(-0.01652V) \tag{13}$$

$$\varepsilon = [1421 - 2.81V]\ (V/cm) \tag{14}$$

Substituting these expressions for the constants into model Eq. (11), our model equation produces the following results:

Table 2
The computational results of P, Q, and ε at three potentiostatic conditions: 450 V, 400 V, and 350 V, at distinct time intervals of 150 s, 100 s, 50 s, and 20 s.

Time (s)	P (mA/cm^2)			Q			ε (V/cm)		
	450 V	400 V	350 V	450 V	400 V	350 V	450 V	400 V	350 V
150	4.18	3.75	3.37	1.57×10^5	2.27×10^5	7.46×10^5	167.24	274.58	448.24
100	4.18	3.75	3.37	1.58×10^5	2.28×10^5	7.48×10^5	167.43	274.84	448.37
50	4.18	3.75	3.37	1.59×10^5	2.30×10^5	7.50×10^5	167.50	274.97	448.50
20	4.18	3.75	3.37	1.50×10^5	2.20×10^5	7.37×10^5	166.34	273.62	447.66

$$J_i = \frac{(0.0081V + 0.5437)\left[exp\,(vZL_{i-1}) - \left(-2.098 \times 10^7\, exp\,(-0.01652V) \times exp\,(-vZL_{i-1})\right)\right]}{exp(vZL_{i-1}) - 1} \tag{15}$$

where $Z = F(1421 - 2.81V)/RT$.

This equation expresses the ionic current density as a function of oxide coating thickness and voltage. We established solutions for the parameters P, Q, and ε across various potentiostatic regimes, advancing similar published work by Ma et al. [4] who expressed the ionic current density as a function of oxide growth in a different metal under a specific potentiostatic condition. This improvement in the equation eliminates the need to run experiments to determine P, Q, and ε for every potentiostatic condition.

Depicting the growth of the oxide coating on Ti during PEO, Eq. (7) describes the reaction rate of the electrode surface ($R_{x,y}$) according to Faraday's law. With the assumption that all Titanium ions participate in the PEO coating and Ti^{4+} serves as the limiting factor for oxide growth (Eqs. (8) and (9)), we provided Eq. (10) that describes the total coating thickness L, and which further indicates that the oxide growth is a function of reaction rate equations 8–10. With the model (Eq. (11)) as proposed by Pyun et al. [5], the ionic current density is established as a function of the oxide thickness equation. Hence, Eqs. 7–11 establish an iterative relationship where the ionic current density is determined from the oxide thickness, and it becomes an input to determine the next oxide thickness Eq. (16).

$$L_i = L_0 + \int_0^t \frac{n_x j_i M_{TiO_2}}{F q_y \rho_{TiO_2}} \tag{16}$$

Plugging in Eq. (15) which is an improvement from Eq. (11) into Eq. (16) provides a means of predicting oxide growth for our system across a range of potentiostatic conditions. In other words, Eq. (16) makes voltage the only input to determine oxide thickness for the PEO of Titanium in our electrolyte.

In Fig. 9, the experimental and simulated oxide growth at different potentiostatic conditions is shown assuming that all Titanium ions participate in the PEO coating. The simulated oxide growth is based on Eq. (16), and it is found that the speed of the oxide thickness growth decreases over the entire treatment time due to the exponential decay of current density under potentiostatic conditions. Also, the oxide coating thickness increases rapidly within the first 10 s because of high current density and then increases slowly due to lower current density at longer treatment times as seen in Fig. 5. Finally, the values of the overall oxide coating thickness calculated by simulation are slightly lower than the values obtained from the experiment under different potentiostatic conditions. This is due to the non-adjustment of porosity in the model, unlike the experimental data that incorporates some porosity. Generally, oxide coating thickness is governed by the currents passing through the coating, the phase formation, and the porosity of the coating. Further research should adjust for porosity when providing simulations for oxide coating thickness.

To confirm that the model can simulate oxide growth at other potentiostatic conditions different from the previously used conditions, we obtained the values for parameters P, Q, and ε at 300 V by solving Eqs. (12)–(14). These values were used as input in Eqs. (11) and (16) to predict the oxide growth. We also experimentally produced PEO coatings of Titanium with similar treatment times under 300 V conditions to verify our prediction. In Fig. 10, the simulated and experimental oxide growth at 300 V is shown displaying similar trends as seen in Fig. 9. The model prediction shows excellent agreement with the experimental observations providing further validation to our model. The present study demonstrates our model's usefulness in predicting oxide growth across a range of potentiostatic conditions. The results show that due to the linear correlation observed in Eqs. (12)–(14), a minimum of two current density decay measurements (from two different voltages) and oxide thickness from experimental data are necessary within a given PEO system to predict oxide thickness for any other specified voltage and time condition for that system.

As noted earlier, modeling of the PEO treatment under potentiostatic conditions is more challenging compared to the galvanostatic case since in the former the current density decays sharply within the first few seconds of processing. Thus, a fast coating growth rate is expected initially that drops substantially with time. On the contrary, in the galvanostatic case, the current density remains constant and as a result, the coating growth rate does not change as much with time. This is demonstrated in Fig. 11 that presents the average coating growth rate as a function of the current density under potentiostatic (current study) versus galvanostatic control using data from PEO of Ti in the same electrolyte from our previous studies [29]. It is clear that a very high growth rate prevails initially in the potentiostatic case that lasts for very short time due to the sharp current decay resulting in relatively thin coatings. Comparatively, in the galvanostatic case, the current density is constant relative to time producing a growth rate that can be maintained for longer time resulting in thicker coatings.

4. Conclusion

We developed an experimentally informed computational model, building upon existing theoretical frameworks, enabling us to predict oxide growth as a function of applied voltage and treatment times during PEO of Titanium in an electrolyte of 0.02 M KOH and 0.01 M $K_4P_2O_7$. By incorporating experimental data into the model, we have successfully captured the interdependency between oxide thickness and ionic current density, providing a versatile tool for predicting coating growth under different potentiostatic conditions.

Data were collected from current density decay and oxide thickness for 450, 400, and 350 V. A linear relationship was discovered between the model parameters and the applied voltage. Based on this model, the oxide growth for an applied potential of 300 V was predicted being in excellent agreement with the experimental measurement.

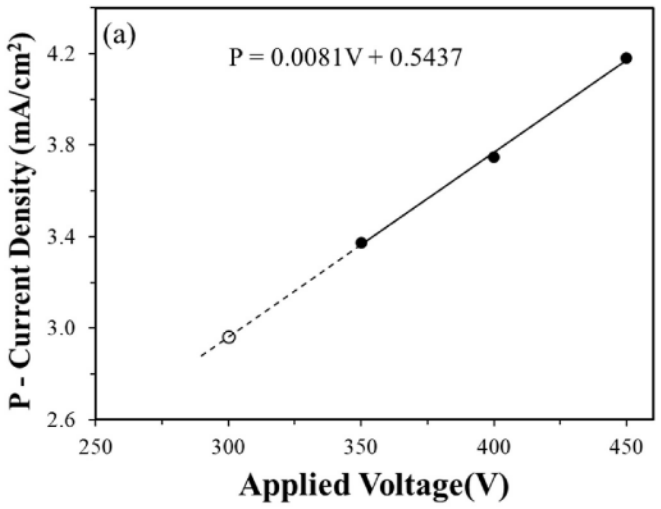

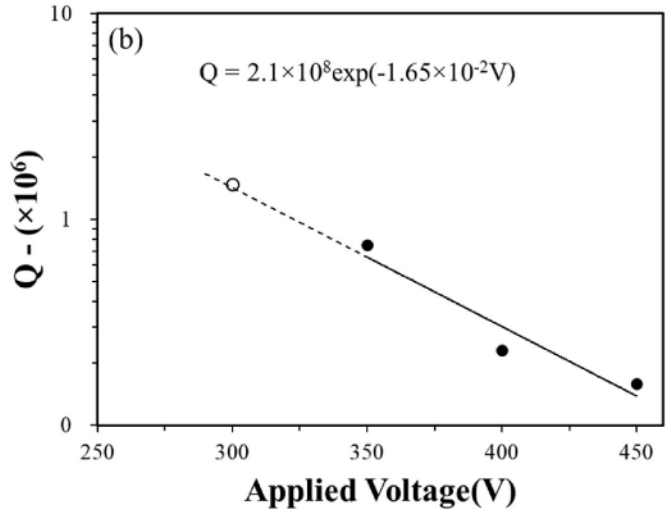

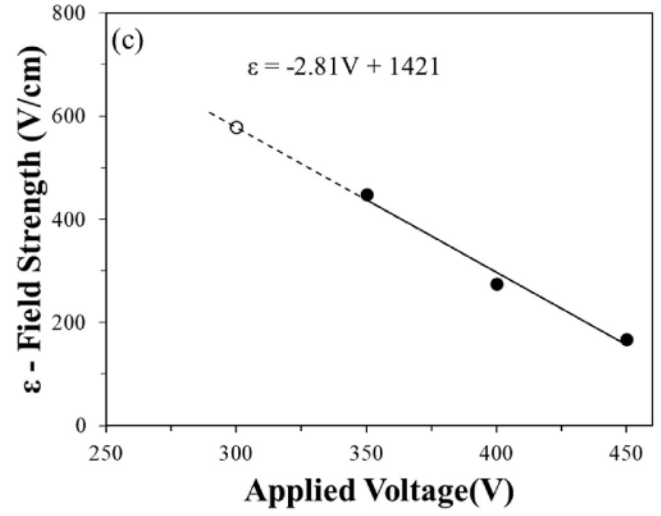

Fig. 8. Optimal solutions for P, Q, and ε corresponding to different potentiostatic conditions with their corresponding line equations.

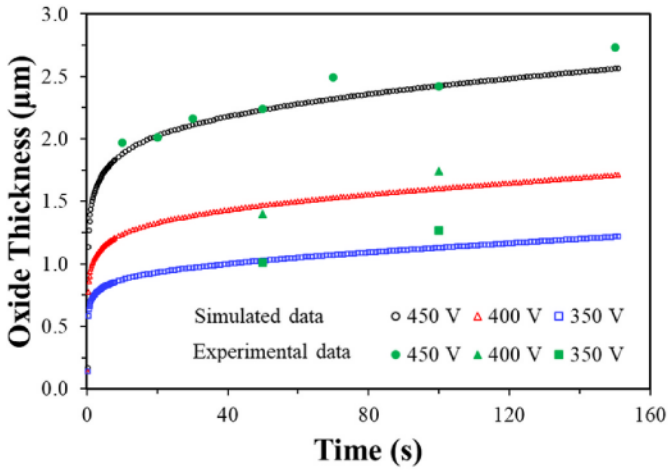

Fig. 9. Simulated oxide growth versus actual oxide growth at different potentiostatic conditions.

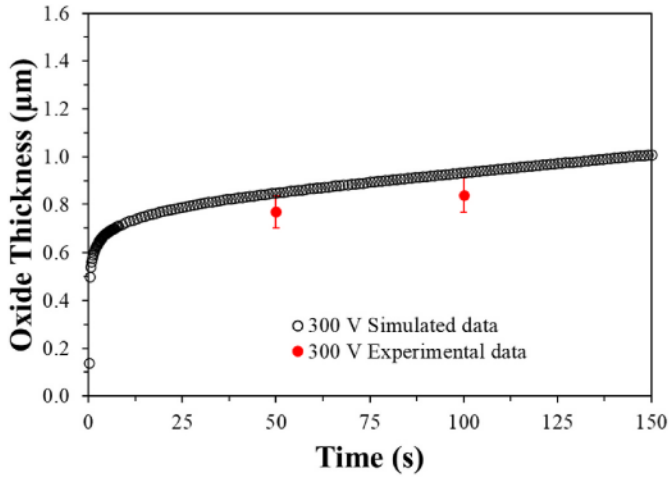

Fig. 10. Simulated oxide growth versus actual oxide growth at 300 V.

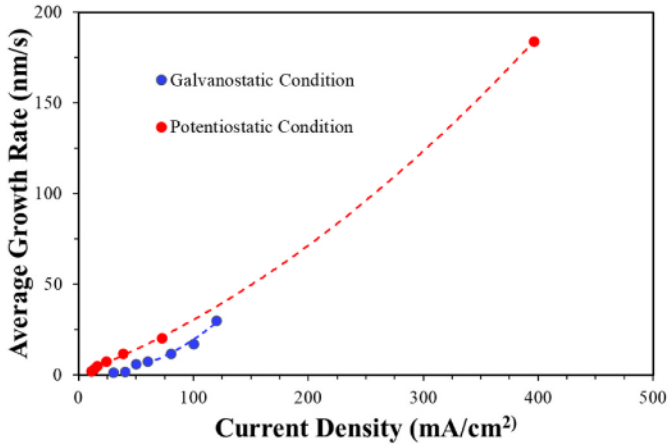

Fig. 11. Average growth rate versus current density for PEO potentiostatic and galvanostatic treatments.

CRediT authorship contribution statement

Kingsley Ochiabuto: Writing – original draft, Software, Methodology, Investigation, Formal analysis, Data curation. **Hunter Pitts:** Investigation. **Ye Cao:** Writing – review & editing, Validation, Formal analysis. **Efstathios Meletis:** Writing – review & editing, Supervision, Funding acquisition, Data curation, Conceptualization.

Declaration of competing interest

The authors declare that they have no known competing financial interests or personal relationships that could have appeared to influence the work reported in this paper.

Data availability

Data will be made available on request.

Acknowledgment

E.I.M. acknowledges the support of the National Science Foundation, Program UTA/NU Paretnership for Research and Education in Materials (NSF DMR-2122128).

References

[1] V. Dehnavi, X.Y. Liu, B.L. Luan, D.W. Shoesmith, S. Rohani, Phase transformation in plasma electrolytic oxidation coatings on 6061 aluminum alloy, Surf. Coating. Technol. 251 (2014/07/25/2014) 106–114, https://doi.org/10.1016/j.surfcoat.2014.04.010.

[2] R. Arrabal, E. Matykina, T. Hashimoto, P. Skeldon, G.E. Thompson, Characterization of AC PEO coatings on magnesium alloys, Surf. Coating. Technol. 203 (16) (2009/05/30/2009) 2207–2220, https://doi.org/10.1016/j.surfcoat.2009.02.011.

[3] A.G. Rakoch, V.V. Khokhlov, V.A. Bautin, N.A. Lebedeva, Y.V. Magurova, I. V. Bardin, Model concepts on the mechanism of microarc oxidation of metal materials and the control over this process, Protect. Met. 42 (2) (2006/03/01 2006) 158–169, https://doi.org/10.1134/S003317320602010X.

[4] X. Ma, C. Blawert, D. Höche, K.U. Kainer, M.L. Zheludkevich, A model describing the growth of a PEO coating on AM50 Mg alloy under constant voltage mode, Electrochim. Acta 251 (2017/10/10/2017) 461–474, https://doi.org/10.1016/j.electacta.2017.08.147.

[5] S.-I. Pyun, M.-H. Hong, A model describing the growth kinetics of passivating oxide film prepared under potentiostatic conditions, Electrochim. Acta 37 (2) (1992/02/01/1992) 327–332, https://doi.org/10.1016/0013-4686(92)85019-H.

[6] J.-P. Caire, F. Dalard, W.S. Minko, Modeling the plasma electrolytic oxidation of aluminium and magnesium alloys, ECS Trans. 2 (13) (2007/02/07 2007) 1, https://doi.org/10.1149/1.2424298.

[7] U. Diebold, The surface science of titanium dioxide, Surf. Sci. Rep. 48 (5–8) (2003) 53–229, https://doi.org/10.1016/S0167-5729(02)00100-0.

[8] A. D. Kashin, M. B. Sedelnikova, P. V. Uvarkin, A. V. Ugodchikova, N. A. Luginin, Y. P. Sharkeev, M. A. Khimich, and O. V. Bakina, "Functionalizing Diatomite-based micro-arc coatings for orthopedic implants: influence of TiO_2 addition," Biomimetics, vol. 8, no. 3, doi: 10.3390/biomimetics8030280.

[9] L.C. Zhang, L.Y. Chen, A review on biomedical titanium alloys: recent progress and prospect, Adv. Eng. Mater. 21 (4) (2019) 1801215, https://doi.org/10.1002/adem.201801215.

[10] H. Bai, L. Zhong, L. Kang, J. Liu, W. Zhuang, Z. Lv, Y. Xu, A review on wear-resistant coating with high hardness and high toughness on the surface of titanium alloy, J. Alloys Compd. 882 (2021) 160645, https://doi.org/10.1016/j.jallcom.2021.160645.

[11] Y. Zhang, F. Chen, Y. Zhang, M. Liu, Y. Pang, C. Du, Microstructure and corrosion resistance of duplex coatings deposited on TC17 alloys by MAO and HiPIMS, Mater. Lett. 303 (2021) 130506, https://doi.org/10.1016/j.matlet.2021.130506.

[12] C.H. Lauro, L.C. Brandão, S.L.M.R. Filho, J.P. Davim, Behaviour of a biocompatible titanium alloy during orthogonal micro-cutting employing green machining techniques, Int. J. Adv. Des. Manuf. Technol. 98 (2018) 1573–1589, https://doi.org/10.1007/s00170-018-2352-8.

[13] J.S. Dhaliwal, S.R.N. David, N.R. Zulhilmi, S.K. Sodhi Dhaliwal, J. Knights, R.F. de Albuquerque Junior, Contamination of titanium dental implants: a narrative review, SN Appl. Sci. 2 (2020) 1–10, https://doi.org/10.1007/s42452-020-2810-4.

[14] A. Palmquist, F. Lindberg, L. Emanuelsson, R. Brånemark, H. Engqvist, P. Thomsen, Morphological studies on machined implants of commercially pure titanium and titanium alloy (Ti6Al4V) in the rabbit, J. Biomed. Mater. Res. B Appl. Biomater. 91 (1) (2009) 309–319, https://doi.org/10.1002/jbm.b.31404.

[15] A. Festas, A. Ramos, J.P. Davim, Machining of titanium alloys for medical application-a review, Proc. IME B J. Eng. Manufact. 236 (4) (2022) 309–318, https://doi.org/10.1177/09544054211028531.

[16] L.-C. Zhang, L.-Y. Chen, L. Wang, Surface modification of titanium and titanium alloys: technologies, developments, and future interests, Adv. Eng. Mater. 22 (5) (2020) 1901258, https://doi.org/10.1002/adem.201901258.

[17] J. Sarma, R. Kumar, A.K. Sahoo, A. Panda, Enhancement of material properties of titanium alloys through heat treatment process: a brief review, Mater. Today: Proc. 23 (2020) 561–564, https://doi.org/10.1016/j.matpr.2019.05.409.

[18] M. Hosseini, S. Sajjadi, M. Momeni, Electrodeposition of platinum metal on titanium and anodised titanium from P salt: application to electro-oxidation of glycerol, Surf. Eng. 23 (6) (2007) 419–424, https://doi.org/10.1179/174329407X260582.

[19] A.A. Adjaottor, E. Ma, E.I. Meletis, On the mechanism of intensified plasma-assisted processing, Surf. Coating. Technol. 89 (3) (1997/03/01/1997) 197–203, https://doi.org/10.1016/S0257-8972(96)02893-9.

[20] T.M. Muraleedharan, E.I. Meletis, Surface modification of pure titanium and Ti_6A1_4V by intensified plasma ion nitriding, Thin Solid Films 221 (1) (1992/12/10/1992) 104–113, https://doi.org/10.1016/0040-6090(92)90802-I.

[21] M. Ali, E. Hamzah, M. Toff, Review of Physical Vapour Deposition (PVD) Techniques Hard Coating, 20, Jurnal Mekanikal, 2005, pp. 42–51.

[22] L. Sun, et al., Chemical vapour deposition, Nat. Rev. Methods Primers 1 (1) (2021/01/14 2021) 5, https://doi.org/10.1038/s43586-020-00005-y.

[23] E.I. Meletis, C.V. Cooper, K. Marchev, The use of intensified plasma-assisted processing to enhance the surface properties of titanium, Surf. Coating. Technol. 113 (3) (1999/03/31/1999) 201–209, https://doi.org/10.1016/S0257-8972(98)00841-X.

[24] J.M. Wheeler, J.A. Curran, S. Shrestha, Microstructure and multi-scale mechanical behavior of hard anodized and plasma electrolytic oxidation (PEO) coatings on aluminum alloy 5052, Surf. Coating. Technol. 207 (2012/08/25/2012) 480–488, https://doi.org/10.1016/j.surfcoat.2012.07.056.

[25] G. Li, F. Ma, P. Liu, S. Qi, W. Li, K. Zhang, X. Chen, Review of micro-arc oxidation of titanium alloys: mechanism, properties and applications, J. Alloys Compd. (2023) 169773, https://doi.org/10.1016/j.jallcom.2023.169773.

[26] M. Aliofkhazraei, D.D. Macdonald, E. Matykina, E.V. Parfenov, V.S. Egorkin, J. A. Curran, S.C. Troughton, S.L. Sinebryuhov, S.V. Gnedenkov, T. Lampke, F. Simchen, H.F. Nabavi, Review of plasma electrolytic oxidation of titanium substrates: mechanism, properties, applications and limitations, Appli. Surface Sci. Adv. 5 (2021) 100121, https://doi.org/10.1016/j.apsadv.2021.100121, 2021/09/01/.

[27] M. Kaseem, S. Fatimah, N. Nashrah, Y.G. Ko, Recent progress in surface modification of metals coated by plasma electrolytic oxidation: principle, structure, and performance, Prog. Mater. Sci. 117 (2021/04/01/2021) 100735, https://doi.org/10.1016/j.pmatsci.2020.100735.

[28] S. Sikdar, P.V. Menezes, R. Maccione, T. Jacob, P.L. Menezes, Plasma electrolytic oxidation (PEO) process—processing, properties, and applications, Nanomaterials 11 (6) (2021) 1375, https://doi.org/10.3390/nano11061375.

[29] G. Mortazavi, J. Jiang, E.I. Meletis, Investigation of the plasma electrolytic oxidation mechanism of titanium, Appl. Surf. Sci. 488 (2019) 370–382, https://doi.org/10.1016/j.apsusc.2019.05.250.

[30] S.V. Gnedenkov, S.L. Sinebryukhov, D.V. Mashtalyar, V.S. Egorkin, A. K. Tsvetnikov, A.N. Minaev, Charge transfer at the antiscale composite layer-electrolyte interface, Protect. Met. 43 (7) (2007/11/01 2007) 667–673, https://doi.org/10.1134/S0033173207070090.

[31] M. Shokouhfar, C. Dehghanian, M. Montazeri, A. Baradaran, Preparation of ceramic coating on Ti substrate by plasma electrolytic oxidation in different electrolytes and evaluation of its corrosion resistance: Part II, Appl. Surf. Sci. 258 (7) (2012/01/15/2012) 2416–2423, https://doi.org/10.1016/j.apsusc.2011.10.064.

[32] H. Jiang, Z. Shao, B. Jing, Effect of electrolyte composition on photocatalytic activity and corrosion resistance of micro-arc oxidation coating on pure titanium, Procedia Earth Planetary Sci. 2 (2011/01/01/2011) 156–161, https://doi.org/10.1016/j.proeps.2011.09.026.

[33] K. Venkateswarlu, N. Rameshbabu, D. Sreekanth, M. Sandhyarani, A.C. Bose, V. Muthupandi, S. Subramanian, Role of electrolyte chemistry on electronic and in vitro electrochemical properties of micro-arc oxidized titania films on Cp Ti, Electrochim. Acta 105 (2013) 468–480, https://doi.org/10.1016/j.electacta.2013.05.032, 2013/08/30/.

[34] J.A. Curran, H. Kalkancı, Y. Magurova, T.W. Clyne, Mullite-rich plasma electrolytic oxide coatings for thermal barrier applications, Surf. Coating. Technol. 201 (21) (2007/08/25/2007) 8683–8687, https://doi.org/10.1016/j.surfcoat.2006.06.050.

[35] P. Bala Srinivasan, J. Liang, R.G. Balajeee, C. Blawert, M. Störmer, W. Dietzel, Effect of pulse frequency on the microstructure, phase composition and corrosion performance of a phosphate-based plasma electrolytic oxidation coated AM50 magnesium alloy, Appl. Surf. Sci. 256 (12) (2010/04/01/2010) 3928–3935, https://doi.org/10.1016/j.apsusc.2010.01.052.

[36] Y. Gao, A. Yerokhin, E. Parfenov, A. Matthews, Application of voltage pulse transient analysis during plasma electrolytic oxidation for assessment of characteristics and corrosion behaviour of Ca- and P-containing coatings on magnesium, Electrochim. Acta 149 (2014/12/10/2014) 218–230, https://doi.org/10.1016/j.electacta.2014.10.063.

[37] A.L. Yerokhin, V. Samsonov, P. Shashkov, A. Pilkington, A. Leyland, A. Matthews, Oxide ceramic coatings on aluminium alloys produced by a pulsed bipolar plasma electrolytic oxidation process, Surf. Coating. Technol. 199 (2) (2005/09/22/2005) 150–157, https://doi.org/10.1016/j.surfcoat.2004.10.147.

[38] K.V. Nadaraia, S.N. Suchkov, I.M. Imshinetskiy, D.V. Mashtalyar, S.L. Sinebrykhov, S.V. Gnedenkov, Some new aspects of the study of dependence of properties of PEO coatings on the parameters of current in potentiodynamic mode, Surf. Coating.

Technol. 426 (2021/11/25/2021) 127744, https://doi.org/10.1016/j.surfcoat.2021.127744.

[39] H. Duan, C. Yan, F. Wang, Effect of electrolyte additives on performance of plasma electrolytic oxidation films formed on magnesium alloy AZ91D, Electrochim. Acta 52 (11) (2007/03/01/2007) 3785–3793, https://doi.org/10.1016/j.electacta.2006.10.066.

[40] F. Liu, D. Shan, Y. Song, E.-H. Han, Effect of additives on the properties of plasma electrolytic oxidation coatings formed on AM50 magnesium alloy in electrolytes containing K2ZrF6, Surf. Coating. Technol. 206 (2) (2011/10/25/2011) 455–463, https://doi.org/10.1016/j.surfcoat.2011.07.054.

[41] I. Imshinetskiy, V. Kashepa, K. Nadaraia, D. Mashtalyar, S. Suchkov, P. Zadorozhny, A. Ustinov, S. Sinebryukhov, and S. Gnedenkov, "PEO coatings modified with halloysite nanotubes: composition, properties, and release performance," Int. J. Mol. Sci., vol. 24, no. 1, doi: 10.3390/ijms24010305.

[42] M.V. Adigamova, I.V. Lukiyanchuk, V.P. Morozova, I.A. Tkachenko, K.N. Kilin, Fe and/or Co-containing coatings on titanium: features of plasma electrolytic formation, composition, and magnetic properties, Surf. Coating. Technol. 446 (2022) 128790, https://doi.org/10.1016/j.surfcoat.2022.128790, 2022/09/25/.

[43] N. Barati, E.I. Meletis, F. Golestani Fard, A. Yerokhin, S. Rastegari, M.A. Faghihi-Sani, Al2O3–ZrO2 nanostructured coatings using DC plasma electrolytic oxidation to improve tribological properties of Al substrates, Appl. Surf. Sci. 356 (2015) 927–934, https://doi.org/10.1016/j.apsusc.2015.08.188, 2015/11/30/.

[44] D. V. Mashtalyar, A.I. Pleshkova, M.A. Piatkova, K.V. Nadaraia, I.M. Imshinetskiy, E.A. Belov, S.N. Suchkov, S.L. Sinebryukhov, and S.V. Gnedenkov, "PTFE-containing coating obtained on Ti by spraying and PEO pretreatment," Coatings, vol. 13, no. 7, doi: 10.3390/coatings13071249.